Article

Synergistic interferon alpha-based drug combinations inhibit SARS-CoV-2 and other viral infections in vitro

Aleksandr Ianevski [1], Rouan Yao [1], Eva Zusinaite [2], Laura Sandra Lello [2], Sainan Wang [2], Eunji Jo [3], Jaewon Yang [3], Hilde Lysvand [1], Kirsti Løseth [1], Valentyn Oksenych [1,9], Tanel Tenson [2], Marc P. Windisch [3], Minna Poranen [4], Anni I. Nieminen [5], Svein Arne Nordbø [1,6], Mona Høysæter Fenstad [1,7], Gunnveig Grødeland [8,9,10], Pål Aukrust [8,9,10], Marius Trøseid [8,9,10], Anu Kantele [11], Andres Merits [2], Magnar Bjørås [1], Denis E. Kainov [1,2,4]*

[1] Department of Clinical and Molecular Medicine (IKOM), Norwegian University of Science and Technology, 7028, Trondheim, Norway
[2] Institute of Technology, University of Tartu, 50411 Tartu, Estonia
[3] Applied Molecular Virology Laboratory, Institut Pasteur Korea, Sampyeong-dong 696, 463-400, Bundang-gu, Seongnam-si, Gyeonggi-do, Korea
[4] Molecular and Integrative Biosciences Research Programme, Faculty of Biological and Environmental Sciences, 00014 University of Helsinki, Finland
[5] Institute for Molecular Medicine Finland, FIMM, University of Helsinki, 00014, Helsinki, Finland
[6] Department of Medical Microbiology, St. Olavs Hospital, 7006, Trondheim, Norway
[7] Department of immunology and transfusion medicine, St. Olavs Hospital, 7006 Trondheim, Norway
[8] Research Institute of Internal Medicine, Oslo University Hospital Rikshospitalet, 0372, Oslo, Norway
[9] Institute of Clinical Medicine (KlinMed), University of Oslo, 0318, Oslo, Norway
[10] Section of Clinical Immunology and Infectious diseases, Oslo University Hospital Rikshospitalet, 0372, Oslo, Norway
[11] Helsinki University Hospital (HUS), University of Helsinki, Helsinki 00290, Finland
*: Correspondence: denis.kainov@ntnu.no; Tel./Fax: +358-405-490-220

Abstract: Antiviral drugs are powerful tools to combat emerging viral diseases, one of the leading causes of morbidity and mortality in the world. However, most existing antivirals have failed to cure COVID-19. Accordingly, there is an urgent need for new therapeutics with powerful antiviral and tolerable side effects. Here, we observed that recombinant human interferon-alpha (IFNa) triggered cell intrinsic and extrinsic antiviral responses and reduced replication of severe acute respiratory syndrome coronavirus 2 (SARS-CoV-2) in human lung epithelial Calu-3 cells. However, IFNa alone was insufficient to completely abolish SARS-CoV-2 replication. The combinations of IFNa with camostat, remdesivir, EIDD-2801, cycloheximide or convalescent serum showed strong synergy and, therefore, effectively inhibited SARS-CoV-2 infection. Additionally, we demonstrated synergistic antiviral activity of IFNa2a with pimodivir against influenza A virus (FluAV) infection in human lung epithelial A549 cells, as well as IFNa2a with lamivudine against human immunodeficiency virus 1 (HIV-1) infection in human TZM-bl cells. Our results indicate that IFNa2a-based combinational therapies help to reduce drug dose and improve efficacy in comparison with monotherapies, making them attractive targets for further pre-clinical and clinical development. Additionally, they have powerful treatment potential, and can be leveraged for use in the inhibition of not only emerging or re-emerging viruses, but also immune-evading or drug-resistant viral variants, and viral co-infections.

Keywords: antivirals; antiviral drug combinations; broad-spectrum antivirals; virus; interferon

1. Introduction

Every year, emerging and re-emerging viruses, such as severe SARS-CoV-2, Middle East respiratory syndrome, Zika virus, Ebola virus, and FluAV, surface from natural reservoirs to infect, disable, and kill people [1, 2]. These outbreaks can be devastating to public health and have the capacity to ruin local and global economies when left untacked. As of January 2021, the emerging outbreak of SARS-CoV-2 has infected nearly 70 million and killed more than 2 million people worldwide. Although dexamethasone has been shown to improve survival in patients with severe or critical COVID-19, there are currently no curative therapies against SARS-CoV-2. According to the World Health Organization, there is an urgent need for better control of emerging and re-emerging viral diseases, including COVID-19.

Recombinant human interferons have been approved as a monotherapy for treatment of hepatitis C virus (HCV) and hepatitis B virus (HBV) infections [3]. They have also been shown to be effective against hepatitis E virus (HEV), hepatitis D virus (HDV), and SARS-CoV-2 in clinical trials, as well as against other viruses in laboratory settings [4-6]. Thus, IFNs can be considered naturally occurring broad-spectrum antivirals.

IFNs are a large class of proteins that trigger a host's innate defense against viruses [7, 8]. IFNs are classified into three groups, according to the cellular receptor they bind. Type I IFNs consist of IFN-alpha (IFNa), IFN-beta (IFNb), IFN-epsilon, IFN-kappa and IFN-omega (IFNw) and bind to the IFN-alpha/beta receptor (IFNAR1/2). Type II IFNs consist of IFN-gamma (IFNg) and interact with IFNGR1/2. Finally, type III IFNs, consisting of IFN-lambda-1/IL29 (IFNl1), IFN-lambda-2/IL28A (IFNl2), IFN-lambda-3/IL28B (IFNl3) and IFN-lambda-4 (IFNl4), pass signals through a receptor complex consisting of interleukin (IL) IL10R2 and IFNLR1 [9].

IFNs induce transcription of interferon-stimulated genes (ISGs), which play a role in intrinsic antiviral and extrinsic immune responses. For example, one such response is activation of Ribonuclease L (RNaseL) that leads to the degradation of viral RNA [10]. In addition, IFNs induce production of interleukins (ILs), C-X-C and C-C motif chemokines (CXCLs and CCLs) and other cytokines to recruit immune cells to the site of infection. Due to their major role in viral immune response, mutations in IFN-signaling pathway genes have resulted in increased susceptibility to viral infections and reduced survival of patients [11-14].

However, IFNs possess limited antiviral efficacy and have side effects when used as monotherapies [15]. Synergistic combinations of several agents can increase effectiveness and overcome toxicities, by countering biological compensation, allowing reduced doses of each compound to be used. Therefore, administration of IFN is often combined with simultaneous treatment with other antivirals (Fig. S1). For example, IFNa plus ribavirin was "golden standard" for treatment of chronic HCV infection for more than decade. A combination of IFNb1b, lopinavir–ritonavir, and ribavirin has been tested for treatment of hospitalized patients with COVID-19 in an open-label, randomized, phase 2 trial [16]. Similarly, IFNa2b and IFNg has also been evaluated in patients positive to SARS-CoV-2 [17]. Both treatments were shown to positively impact the resolution of the COVID-19 symptoms.

Here, we present several novel synergistic drug combinations that were achieved by combining IFNa2a with known approved or investigational antiviral agents. We demonstrate that combinations of IFNa2a with camostat, EIDD-2801, remdesivir, cycloheximide, or convalescent serum were synergistic against SARS-CoV-2 infection in human non-small cell lung cancer Calu-3 cells. Additionally, we show that IFNa2a and pimodivir exhibit antiviral synergism against FluAV infection in human adenocarcinoma alveolar basal epithelial A549 cells, and that IFNa2a and lamivudine exhibit synergy against HIV-1 infection in human cervical cancer derived TZM-bl cells. These combinations were effective at lower concentrations compared to monotherapies; therefore, we present them here as treatment options that warrant further investigation.

2. Materials and Methods

2.1. Drugs

Lyophilized recombinant human IFNa1b (cat #: 11343594), IFNa2a (cat #: 11343504), IFNa2b (cat #: 11343514), IFNb1a (cat #: 11343520), IFNb1b (cat #: 11343542), IFNg (cat #: 11343534), IFNw1 (cat #: 11344784), IL28A (cat #: 11340280), and IL-29 (cat #: 11340290) were obtained from ImmunoTools, Germany. IFNs were dissolved in sterile deionized water to obtain 200 μg/mL concentrations. The convalescent serum (G614) obtained from a recovered COVID-19 patient has been described in a previous study [18]. The small molecule drugs camostat (cat #:16018), remdesivir (cat #: 30354), lamivudine (cat #: S1706), cycloheximide (cat #: C7698-1g), pimodivir (cat #: HY-12353A/CS) and EIDD-2801 (cat #: HY-135853) were purchased from Cayman Chemicals, Selleckchem, SigmaAldrich, or MedChemExpress. To obtain 10 mM stock solutions, compounds were dissolved in dimethyl sulfoxide (DMSO; Sigma-Aldrich, Hamburg, Germany) or milli-Q water. The reagents were stored at −80 °C.

2.2. Cells

Human non-small cell lung cancer Calu-3 cells were grown in DMEM-F12 supplemented with 10% FBS, 100 μg/mL streptomycin, and 100 U/mL penicillin (Pen–Strep). Human adenocarcinoma alveolar basal epithelial A549 and African green monkey kidney Vero-E6 cells were grown in DMEM supplemented with 10% FBS and Pen–Strep. ACH-2 cells, which possess a single integrated copy of the provirus HIV-1 strain LAI (NIH AIDS Reagent Program), were grown in RPMI-1640 medium supplemented with 10% FBS and Pen–Strep. TZM-bl, previously designated JC53-bl (clone 13) is a human cervical cancer HeLa cell line. The cells express firefly luciferase under control of HIV-1 long terminal repeat (LTR) promoter allowing quantitation of the viral infection (tat-protein expression by integrated HIV-1 provirus) using firefly luciferase assay. TZM-bl cells were grown in DMEM supplemented with 10% FBS and Pen/Strep. Madin-Darby Canine Kidney (MDCK) cells in DMEM containing Pen/Strep, 0.2% bovine serum albumin, 2 mM l-glutamine, and 1 μg/mL l-1-tosylamido-2-phenylethyl chloromethyl ketone-trypsin (TPCK)-trypsin (Sigma-Aldrich, St. Louis, USA). All cell lines were grown in a humidified incubator at 37 °C in the presence of 5% CO_2.

2.3. Viruses

The wild-type SARS-CoV-2 (hCoV-19/Norway/Trondheim-S15/2020) and recombinant mCherry-expressing SARS-CoV-2 strains (SARS-CoV-2-mCherry) used in this study have been described previously [18] (Rihn et al., PBIOLOGY-D-20-02646R2). Viruses were amplified in a monolayer of Vero-E6 cells in DMEM media containing Pen–Strep and 0.2% bovine serum albumin. Wild type human influenza A/Udorn/307/1972 (H3N2) was amplified in a monolayer of MDCK cells. To produce HIV-1, 6×10^6 ACH-2 cells were seeded in 10 mL medium. Virus production was induced by the addition of 100 nM phorbol-12-myristate-13-acetate. The cells were incubated for 48 h, and the HIV-1-containing medium was collected. The amount of HIV-1 was estimated by measuring p24 levels in the medium using an anti-p24-ELISA, which was developed in-house. Recombinant purified p24 protein was used as a reference. All virus stocks were stored at −80 °C.

2.4. Drug Testing and Drug Sensitivity Quantification

Approximately 4×10^4 Vero-E6 or Calu-3 cells were seeded per well in 96-well plates. The cells were grown for 24 h in DMEM or DMEM-F12, respectively, supplemented with 10% FBS and Pen–Strep. The medium was then replaced with DMEM or DMEM-F12 containing 0.2% BSA, Pen–Strep and the compounds in 3-fold dilutions at 7 different concentrations. No compounds were added to the control wells. The cells were uninfected (mock) or infected with SARS-CoV-2 or SARS-CoV-2-mCherry strains at a multiplicity of infection (moi) of 0.01. After 72 h of infection, a CellTiter-Glo (CTG) assay was performed

to measure cell viability. Drug efficacy on SARS-CoV-2-mCherry infected cells was measured on PFA- or acetone-fixed cells with fluorescence.

For testing compound toxicity and efficacy against FluAV, approximately 4×10^4 A549 cells were seeded in each well of a 96-well plate. The cells were grown for 24 h in growth medium in DMEM supplemented with 10% FBS and Pen–Strep. The medium was then replaced with DMEM containing 0.2% BSA, Pen–Strep, 0,5 μg/mL TPSK-trypsin and compounds in three-fold dilutions at seven different concentrations. No compounds were added to the control wells. The cells were infected with FluAV (moi = 0.5) or mock. At 48 hpi, the media was removed, and a CTG assay was performed to measure cell viability.

For testing compound toxicity and efficacy against HIV-1, approximately 4×10^4 TZM-bl cells were seeded in each well of a 96-well plate in growth medium in DMEM supplemented with 10% FBS and Pen–Strep. The cells were grown for 24 h in growth medium. The medium was then replaced with DMEM containing 0.2% BSA, Pen–Strep and the compounds in 3-fold dilutions at 7 different concentrations. No compounds were added to the control wells. The cells were infected with HIV-1 (corresponding to 300 ng/mL of HIV-1 p24) or mock. At 48 hours post-infection (hpi), the media was removed from the cells, the cells were lysed, and firefly luciferase activity was measured using the Luciferase Assay System (Promega, Madison, WI, USA). In a parallel experiment, a CTG assay was performed to measure cell viability.

The half-maximal cytotoxic concentration (CC_{50}) for each compound was calculated based on viability/death curves obtained on mock-infected cells after non-linear regression analysis with a variable slope using GraphPad Prism software version 7.0a. The half-maximal effective concentrations (EC_{50}) were calculated based on the analysis of the viability of infected cells by fitting drug dose-response curves using four-parameter (*4PL*) logistic function *f(x)*:

$$f(x) = A_{min} + \frac{A_{max} - A_{min}}{1 + (\frac{x}{m})^{\lambda}}, \quad (1)$$

where $f(x)$ is a response value at dose x, A_{min} and A_{max} are the upper and lower asymptotes (minimal and maximal drug effects), m is the dose that produces the half-maximal effect (EC_{50} or CC_{50}), and λ is the steepness (slope) of the curve. The relative effectiveness of the drug was defined as selectivity index (*SI* = CC_{50}/EC_{50}).

To quantify each drug responses in a single metric, a drug sensitivity score (*DSS*) was calculated as a normalized version of standard area under dose-response curve (*AUC*), with the baseline noise subtracted, and normalized maximal response at the highest concentration (often corresponding to off-target toxicity):

$$DSS = \frac{AUC - t(x_{max} - x_{min})}{(100 - t)(x_{max} - x_{min}) \log_{10} Amin}, \quad (2)$$

where activity threshold t equals 10%, and DSS $\in$ [0,50].

2.5. Drug Combination Test and Synergy Calculations

Calu-3, A549 or TZM-bl cells were treated with different concentrations of two drugs and infected with SARS-CoV-2-mCherry (moi = 0.01), FluAV (moi = 0.5), HIV-1 (corresponding to 300 ng/mL of HIV-1 p24) or mock. After 48 h, reporter protein expression (SARS-CoV-2-mCherry and HIV-1) and cell viability were measured as described above. To test whether the drug combinations act synergistically, the observed responses were compared with expected combination responses. The expected responses were calculated based on the ZIP reference model using SynergyFinder version 2 [19, 20]. Final synergy scores were quantified as average excess response due to drug interactions (i.e., 10% of cell survival beyond the expected additivity between single drugs represents a synergy score of 10). Additionally, for each drug combination, we report a most synergistic area score – the most synergistic 3-by-3 dose-window in a dose-response matrix.

2.6. Plaque assay

To quantitate the production of infectious virions, we titered SARS-CoV-2 viruses amplified in IFN-treated and untreated cells. Media from the viral culture were serially diluted from 10^{-2} to 10^{-7} in DMEM containing 0.2% BSA. The dilutions were applied to a monolayer of Vero-E6 cells in 24-well plates. After one hour, cells were overlaid with virus growth medium containing 1% carboxymethyl cellulose and incubated for 72 h. The cells were fixed and stained with crystal violet dye, and the plaques were calculated in each well and expressed as plaque-forming units per mL (pfu/mL).

2.7. Gene Expression Analysis

Calu-3 cells were treated with 1 μg/ml IFNa2a or vehicle control. Cells were infected with SARS-CoV-2-mCherry at a moi of 0.01 or mock. After 24 h, total RNA was isolated using RNeasy Plus Mini kit (Qiagen, Hilden, Germany). Polyadenylated mRNA was isolated from 250 ng of total RNA with NEBNext Poly(A) mRNA magnetic isolation module. NEBNext Ultra II Directional RNA Library Prep kit from Illumina was used to prepare samples for sequencing. Sequencing was done on NextSeq 500 instrument (set up: single-end 1 x 76 bp + dual index 8 bp) using NextSeq High Output 75 cycle sequencing kit (up to 400M reads per flow cell). Reads were aligned using the Bowtie 2 software package version 2.4.2 to the NCBI reference sequence for SARS-CoV-2 (NC_045512.2) and to the human GRCh38 genome. *The n*umber of mapped and unmapped reads that aligned to each gene were obtained with the featureCounts function from Rsubread R-package version 2.10. The GTF table for the reference sequence was downloaded from https://ftp.ncbi.nlm.nih.gov/genomes/all/GCF/009/858/895/GCF_009858895.2_SM985889v3/GCF_009858895.2_ASM985889v3_genomic.gtf.gz. The heatmaps were generated using the pheatmap package (https://cran.r-project.org/web/packages/pheatmap/index.html) based on log2-transformed profiling data.

2.8. Metabolic Analysis

Calu-3 cells were treated with 1 μg/ml IFNa2a or vehicle control. Cells were infected with SARS-CoV-2-mCherry at a moi 0.01 or mock. After 24 h, virus was inactivated with UVC radiation and trypsin treatment as described previously [18].

Metabolites were extracted from 100 μl of cell culture medium with 400 μL of cold extraction solvent (acetonitrile:methanol:water; 40:40:20). Subsequently, samples were sonicated for 3 cycle (60 s, power = 60 and frequency = 37), vortexed for 2 min and centrifuged at 4 °C, 14000 rpm for 10 min. The supernatant was transferred to autosampler vials for LC-MS analysis. The extracts were analyzed with Thermo Vanquish UHPLC+ system coupled to a QExactive Orbitrap quadrupole mass spectrometer equipped with a heated electrospray ionization (H-ESI) source probe (Thermo Fischer Scientific, Waltham, MA, USA). A SeQuant ZIC-pHILIC (2.1 × 100 mm, 5 μm particles) HILIC phase analytical column (Merck KGaA, Darmstadt, Germany) was used as a chromatographic separation column.

Gradient elution was carried out with a flow rate of 0.100 mL/min with 20 mM ammonium carbonate, adjusted to pH 9.4 with ammonium solution (25%) as mobile phase A and acetonitrile as mobile phase B. The gradient elution was initiated from 20% mobile phase A and 80% mobile phase B and maintained for 2 min. Then, mobile phase A was gradually increased up to 80% for 17 min, followed by a decrease to 20% over the course of 17.1 min. and sustained for up to 24 min.

The column oven and auto-sampler temperatures were set to 40 ± 3 °C and 5 ± 3 °C, respectively. The mass spectrometer was equipped with a heated electrospray ionization (H-ESI) source using polarity switching and the following settings: resolution of 35,000, the spray voltages of 4250 V for positive and 3250 V for negative mode, sheath gas at 25 arbitrary units (AU), the auxiliary gas at 15 AU, sweep gas flow of 0, Capillary temperature of 275°C, and S-lens RF level of 50.0. Instrument control was operated

with Xcalibur 4.1.31.9 software (Thermo Fischer Scientific, Waltham, MA, USA). Metabolite peaks were confirmed using the mass spectrometry metabolite library kit MSMLS-1EA (Sigma Aldrich supplied by IROA Technologies).

In the data processing, the final peak integration was done with the TraceFinder 4.1 software (Thermo Fisher Scientific, Waltham, MA, USA) and for further data analysis, the peak area data was exported as an Excel file. Data quality was monitored throughout the run using pooled healthy human serum as Quality Control (QC), which was processed and extracted in the same manner as unknown samples. After integration of QC data with TraceFinder 4.1, each detected metabolite was checked and %RSD were calculated, while the acceptance limit was set to ≤ 20%.

Blank samples were injected after every five runs to monitor any metabolite carryover. A carryover limit of ≤ 20% was set for each metabolite. Percentage background noise was calculated by injecting a blank sample at the beginning of the run. The acceptance limit for background noise was set at ≤ 20% for each metabolite.

3. Results

3.1. Type I IFNs reduce SARS-CoV-2 replication in vitro more efficiently than type II and III IFNs

To date, there are still no potently effective antiviral therapies available to treat COVID-19 patients. However, previous studies have uncovered several potent antiviral agents including IFNs against SARS-CoV-2 in vitro and in vivo [4, 5, 18]. Here, we tested type I, II, and III IFNs against wild type SARS-CoV-2 in Calu-3 and Vero-E6 cells using cell viability and virus plaque reduction assays as readouts. We observed that type I IFNs rescued both cell types from virus-mediated death and reduced SARS-CoV-2 replication more efficiently than type II and III IFNs. However, the rescue was only partial, and virus replication was reduced only by 2-3-folds (Fig. 1).

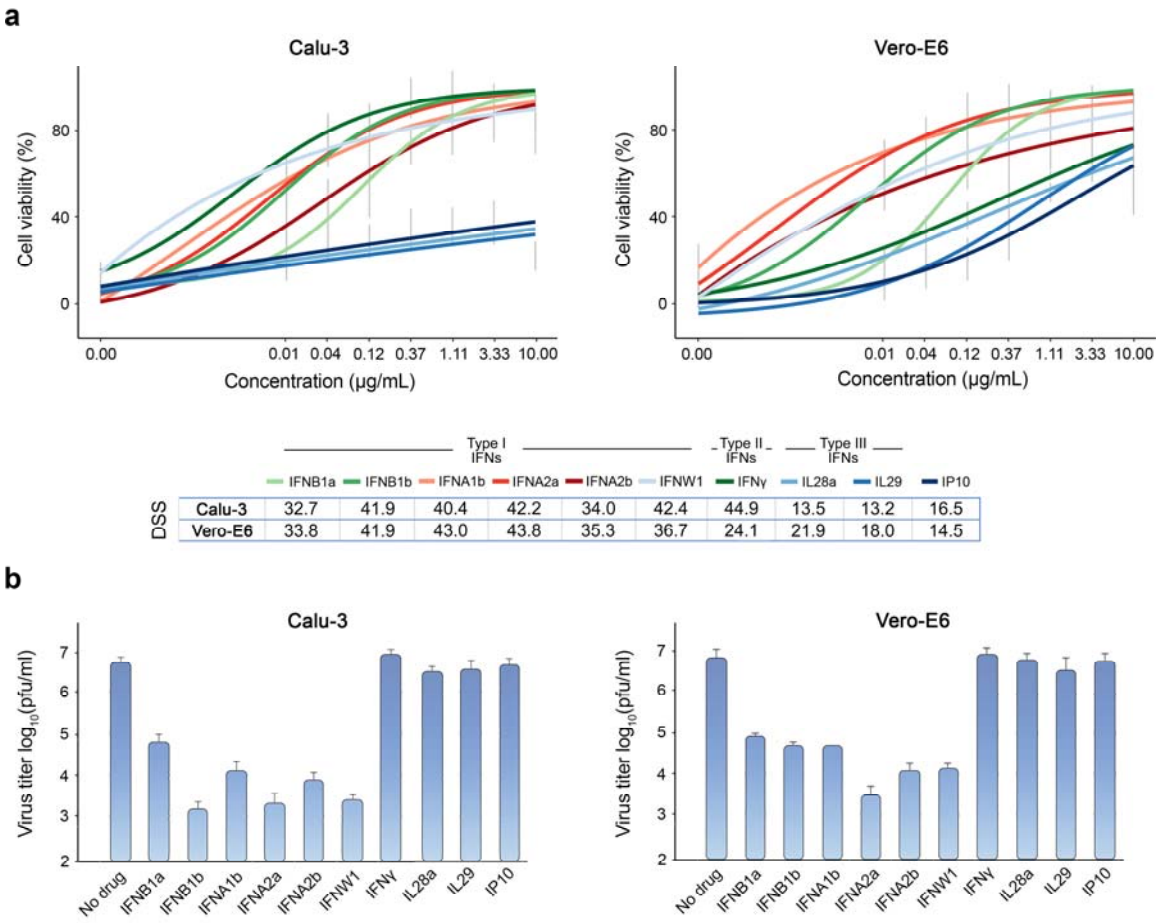

Figure 1. Type I IFNs rescue Calu-3 and Vero-E6 cells from SARS-CoV-2-mediated death and attenuate virus replication. (**a**) The effect of different doses of IFNs on viability of SARS-CoV-2-infected (moi = 0.01) Calu3 and Vero-E6 cells. Cell viability was determined using the CTG assay at 72 hpi. Mean ± SD; n = 3. The anti-SARS-CoV-2 activity of the IFNs was quantified using drug sensitivity scores (DSS). (**b**) The effects of IFNs on viral replication, measured by plaque reduction assay. Mean ± SD; n = 3.

3.2. Type I IFNs reduce the SARS-CoV-2 RNA replication and accelerate virus-mediated induction of cellular type III IFNs, IFNb1 and ISGs

To shed more light on the mechanism of action of type I IFNs, we evaluated their effect on expression of cellular genes and transcription of viral RNA in mock- and SARS-CoV-2-infected Calu-3 cells. For this, cells were treated with 1 µg/mL of type I IFNs or vehicle and infected with virus or mock. After 24 h, we analyzed polyadenylated RNA using RNA-sequencing. We found that type I IFNs attenuated production of viral RNA (Fig. 2a), while increasing expression of many ISGs in both mock- and virus-infected cells (Fig. 2b). These include IFIT1, IFIT2 and IFIT3, which play a role in recognition of viral RNA; OASL and OAS2, which are involved in RNase L-mediated RNA degradation; and IDO1 which is essential for kynurenine biosynthesis [21-24]. Interestingly, type I IFNs boosted virus-activated expression of type III IFNs (IFNl1, IFNl2, IFNl3 and IFNl4) as well as IFNb1, which belongs to type I IFN. These results indicate that type I IFNs not only trigger expression of ISGs regardless of infection, but also amplify expression of other interferons usually activated by viral infections.

Next, we studied the effect of type I IFNs on the metabolism of mock- and SARS-CoV-2 -infected Calu-3 cells. We analyzed mainly polar metabolites in cell cultures at 24 hpi (Fig. S2; Fig. S2). A total of 93

metabolites were quantified. Viral infection substantially lowered tyrosine and 4-hydroxyproline levels ($log_2FC<-2$). Regardless of viral infection, administration of type I IFNs lowered the levels of several metabolites including tryptophan while increasing kynurenine ($log_2FC>3$; Fig. 2c). This indicates that type I IFNs activate IDO1-mediated kynurenine biosynthesis, which is responsible for adverse reactions such as suppression of T-cell responses, pain hypersensitivity and behavior disturbance [25].

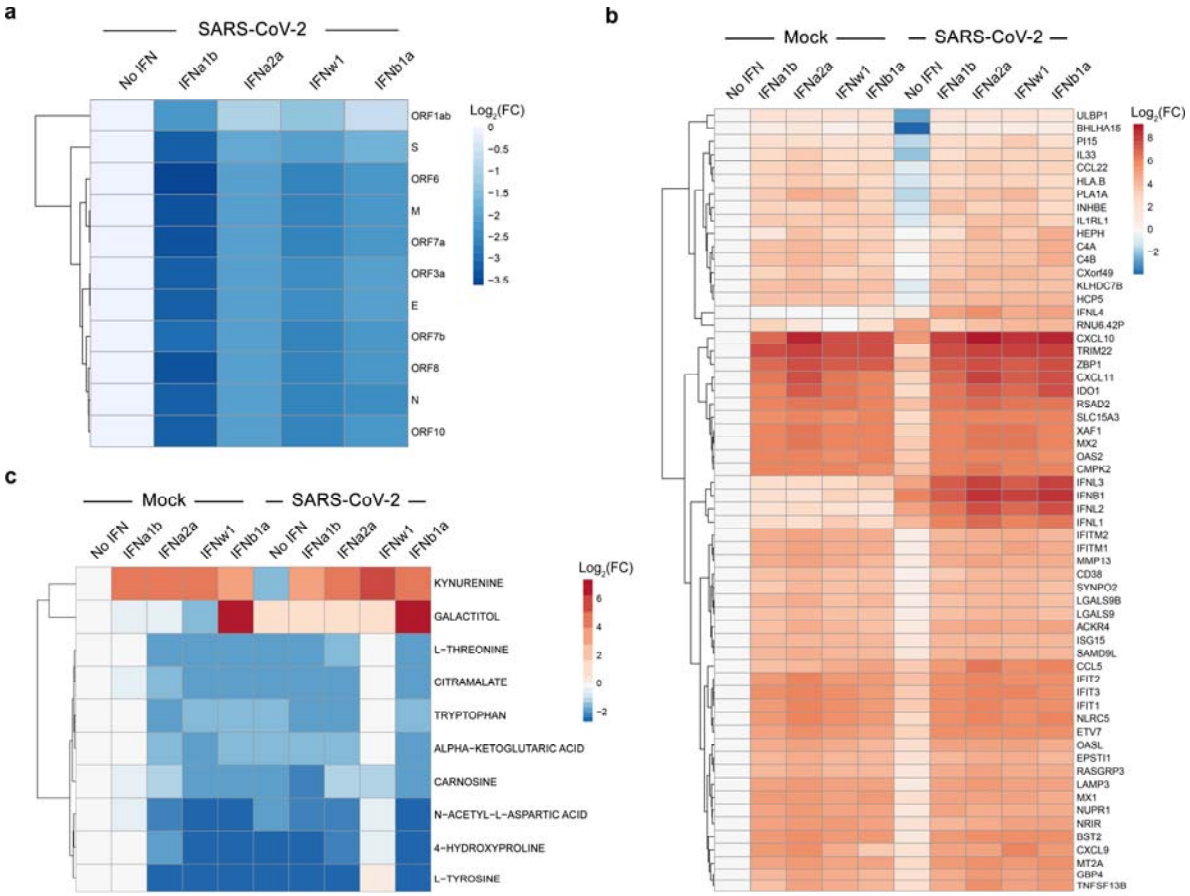

Figure 2. Transcriptomic and metabolomic analysis of mock- and SARS-CoV-2-infected Calu-3 cells non-treated or treated with type I IFNs. (**a**) Calu-3 cells were stimulated with IFNs (1 µg/mL) or non-stimulated and infected with SARS-CoV-2 (moi = 0,01). A heatmap of viral RNAs affected by treatment is shown. Each cell is colored according to the log2-transformed expression values of the samples, expressed as fold-change relative to the nontreated control. (**b**) Calu-3 cells were either stimulated with purified recombinant human IFN (1 µg/mL) or left untreated with IFN, then infected with either mock or SARS-CoV-2 (moi = 0,01). A heatmap of the most variable cellular genes affected by treatment and virus infection is shown. Each cell is colored according to the log2-transformed expression values of the samples, expressed as fold-change relative to the nontreated mock-infected control. (**c**) Cells were treated as for panel b. After 24 h, the cell culture supernatants were collected, and metabolite levels were determined by LC-MS/MS. A heatmap of the most affected metabolites is shown. Each cell is colored according to the log2-transferred profiling values of samples, expressed as fold-change relative to the mock control.

3.3. IFNa1b, IFNa2a and IFNw1 are more effective than IFNb1a against SARS-CoV-2 in Calu-3 cells

To identify the type I IFN with most activity against SARS-CoV-2 infection, we infected IFN-treated and IFN-untreated Calu-3 cells with SARS-CoV-2-mCherry (moi 0.01) and collected media from the cells (P1) after 48 h. The media were diluted 25-fold and applied to noninfected cells for another 48 h (P2).

Mock-infected cells were used as controls. The experiment is schematically depicted in Fig. 3a. Fluorescent microscopy, fluorescence intensity analysis and cell viability assay of P1 and P2 cells showed that IFNa1b, IFNa2a and IFNw1 were more effective inhibitors of SARS-CoV-2 infection than IFNb1a. However, none of the IFNs tested able to inhibit virus infection completely (Fig. 3b-d).

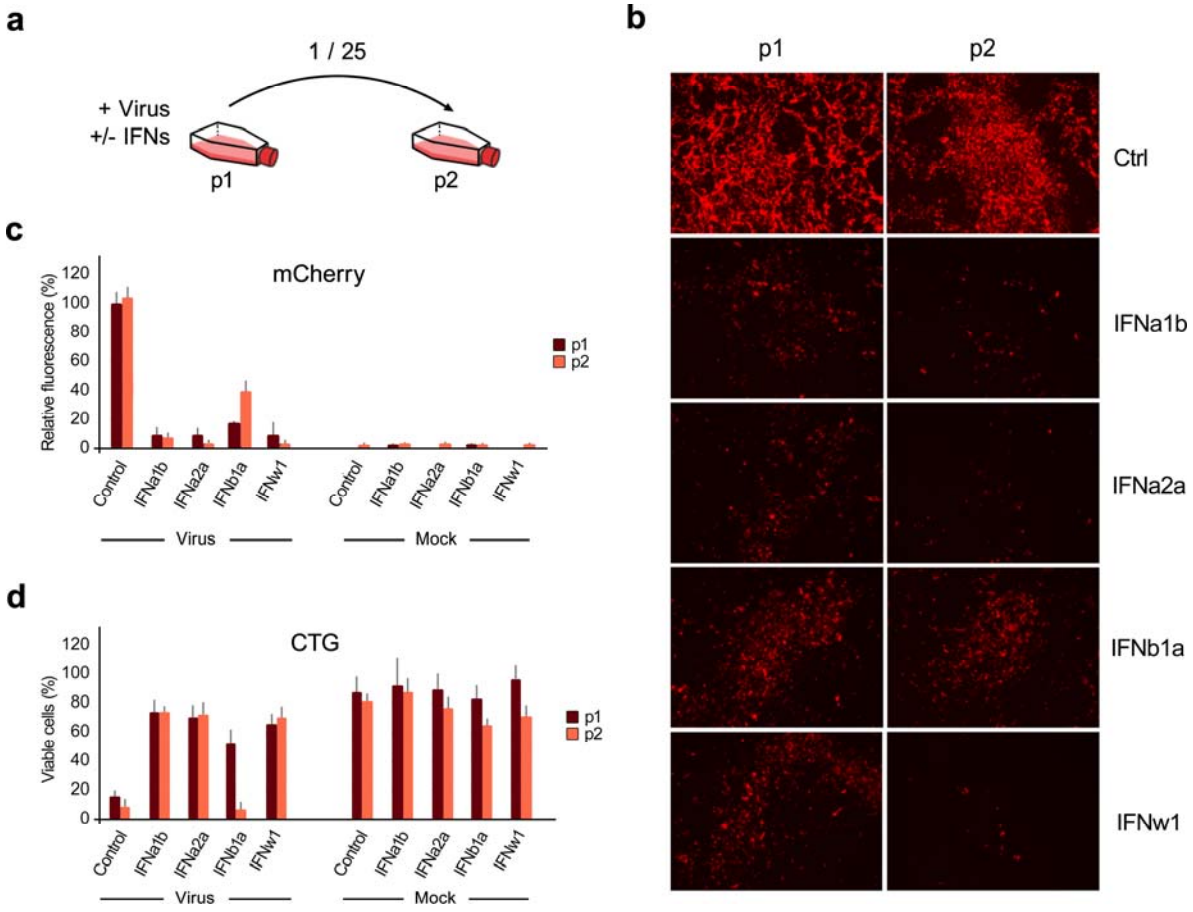

Figure 3. IFNa1b, IFNa2a and IFNw1 are more effective than IFNb1a against SARS-CoV-2-mCherry infection in Calu-3 cells. (**a**) Schematic representation of the experimental setup. (**b**) Fluorescent images of non-treated (Ctrl) and IFN-treated (1 µg/mL) SARS-CoV-2-mCherry-infected Calu-3 cells (P1) and cells (P2) treated with 25-fold diluted media from P1 cells taken at 48 hpi. (**c, d**) Fluorescence intensity and viability analysis of P1 and P2 cells performed at 48 hpi. Mock-infected cells were used as controls (Mean ± SD; n = 3).

3.4. Anti-SARS-CoV-2 activity of IFNa2a depends on virus load and time of addition

The IFNas are widely used in basic research to elucidate biological activities, structure and mechanism of action of type I IFNs. The IFNas are encoded by multiple genes resulting in slightly different proteins. We tested IFNa2a against various doses of SARS-CoV-2-mCherry in Calu-3 cells. Calu-3 cells were treated with 1 µg/mL IFNa2a, then infected with SARS-CoV-2-mCherry at indicated moi. After 48 h, fluorescent intensity and cell viability analysis were performed. We found that efficacy of IFNa2a treatment in preventing SARS-CoV-2 infection was dependent on virus load, decreasing in efficacy as moi increases (Fig. 4a).

We also tested whether time of IFNa2a addition could influence its anti-SARS-CoV-2 activity. To this end, we treated Calu-3 cells with 1 µg/mL IFNa2a at indicated time points and infected the cells with SARS-CoV-2-mCherry (moi = 0.01). After 48 h of infection, fluorescent intensity and cell viability analysis were performed.

We found that efficacy of IFNa2a treatment was dependent on time of administration, shown more efficacy when given prior virus infection than following infection (Fig. 4b).

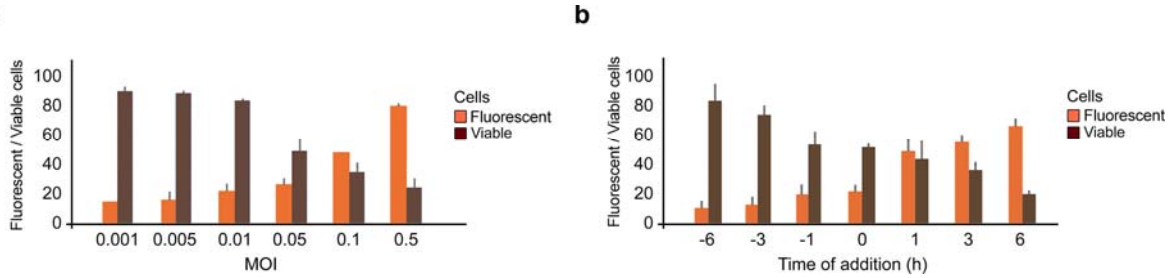

Figure 4. Anti-SARS-CoV-2 activity of IFNa2a depends on moi and time of administration. (**a**) Calu-3 cells were treated with 1 μg/mL IFNa2a and infected with indicated moi of SARS-CoV-2-mCherry. Fluorescent intensity and cell viability were measured after 48 h (Mean ± SD; n = 3). (**b**) Calu-3 cells were treated with 1 μg/mL IFNa2a prior, simultaneously or post infection with SARS-CoV-2-mCherry (moi 0.01). Fluorescent intensity and cell viability were measured after 48 h (Mean ± SD; n = 3).

3.5. Synergistic IFNa2a-based Combinations Against SARS-CoV-2 infection

Next, we examined whether combinations of IFNa2a with several known inhibitors of SARS-CoV-2 infection can protect cells from virus infection more efficiently than IFNa2a alone. For this, we first confirmed antiviral activities of remdesivir, EIDD-2801, camostat, cycloheximide, and convalescent serum [26-30] on Calu-3 cells using SARS-CoV-2-mCherry (Fig. S3). Then we tested the antiviral efficacy of these agents in combination with IFNa2a in Calu-3 cells by monitoring virus-mediated mCherry expression and cell viability. Each drug combination was tested in a 6×6 dose-response matrix, where 5 doses of single drugs are combined in a pairwise manner. As a result, we obtained dose-response matrices demonstrating virus inhibition and cell viability achieved by each combination (Fig 5a,b; Fig. S4). We plotted synergy distribution maps, showing synergy at each pairwise dose. For each drug combination, we calculated ZIP synergy scores and most synergistic area scores (Fig. 5c). We observed that all combinations were synergistic based on fluorescent intensity or cell viability analyses (synergy scores >10). However, camostat-IFNa2a and convalescent plasma-IFNa2a were the most active in terms of both dose-response effect and synergism. This high synergy allowed us to substantially decrease the concentration of both components (especially IFNa2a) to achieve antiviral efficacy that was comparable to those of individual drugs at high concentrations.

Based on our transcriptomics and metabolomics analysis of anti-SARS-CoV-2 activity of IFNa2a and literature review on remdesivir, EIDD-2801, camostat, cycloheximide, and convalescent serum, we propose the following mechanism of action of the drug combinations. Fig. 6d shows that IFNa2a induces transcription of ISGs including IFIT1, IFIT2 and IFIT3, which recognize viral RNA; OASL and OAS2, which are involved in RNase L-mediated RNA degradation; and IDO1, which catalyzes kynurenine biosynthesis. IFNa2a also facilitates expression of several cytokines and virus-activated synthesis of IFNL1, IFNL2, IFNL3, IFNL4, and IFNB1, which alarm the neighboring cells of upcoming infection. Convalescent serum contains neutralizing antibodies which bind S protein of SARS-CoV-2 preventing virus entry into the cells [16]. Camostat, a serine protease inhibitor, reduces SARS-CoV-2-cell membrane fusion by binding host TMPRSS2 [31]. Remdesivir and EIDD-2801 are nucleoside analogues which inhibit viral RNA synthesis [28, 32]. Cycloheximide inhibits translation elongation and, thereby, reduces SARS-CoV-2 replication [27]. Thus, a combination of therapies that works to bolster innate immune response while targeting viral entry or replication may work together to inhibit infection within a virus-host system. These combinations lowered toxicity and improved efficacy in comparison with monotherapies in vitro, making them attractive targets for further pre-clinical and clinical development.

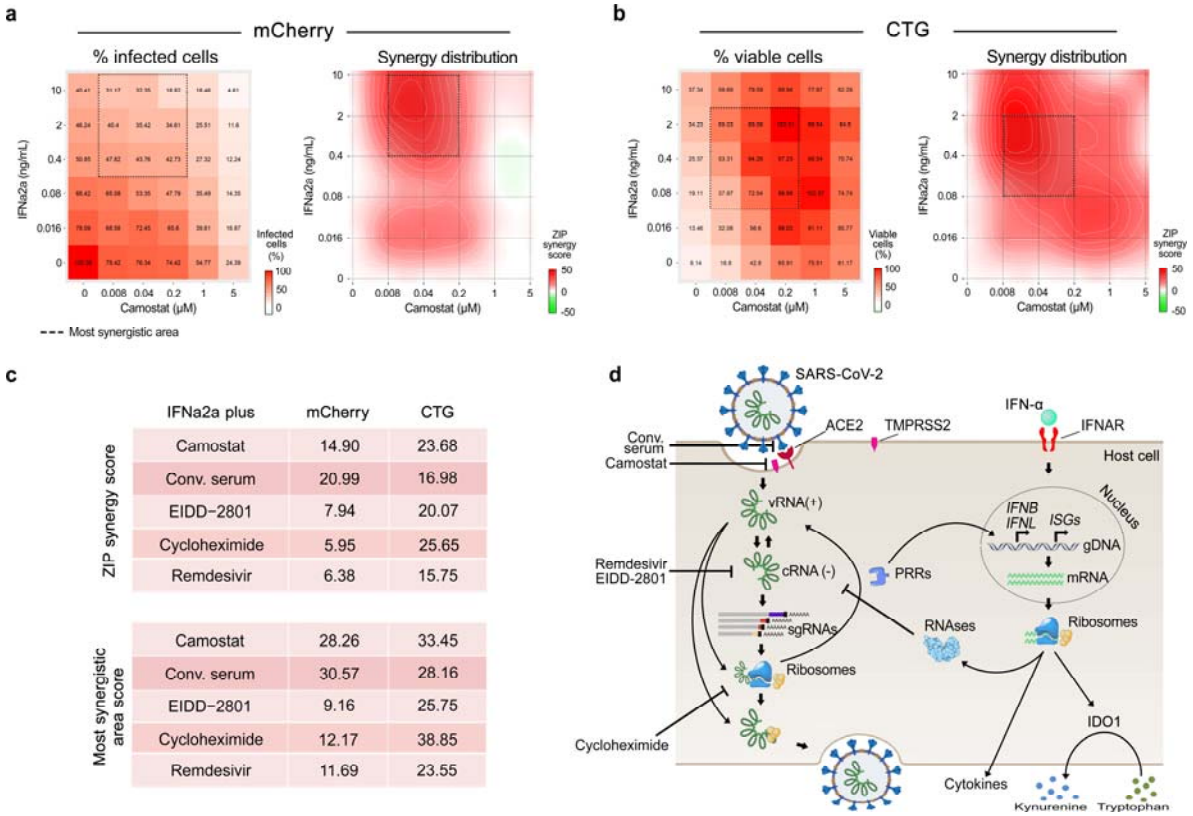

Figure 5. Synergistic IFNa2a-based combinations against SARS-CoV-2-mCherry infection in Calu-3 cells. (**a**) The interaction landscape of IFNa2a and camostat in SARS-CoV-2-mCherry infected Calu-3 cells measured using fluorescence (left panel). The interaction landscape of both drugs showing synergy of the drug combination (right panel). (**b**) The interaction landscapes of IFNa2a and camostat in SARS-CoV-2-mCherry infected Calu-3 cells measured using CTG (left panel). The interaction landscape of both drugs showing synergy of the drug combination (right panel). (c) ZIP synergy scores (synergy score for whole 6×6 dose-response matrices) and the most synergistic area scores (synergy score for most synergistic 3×3 dose-regions) calculated for indicated drug combinations. (d) Schematic representation of mechanisms of anti-SARS-CoV-2 actions of remdesivir, EIDD-2801, camostat, cycloheximide, and convalescent serum, and stages of virus replication cycle they target.

3.6. Novel IFNa2a-based Combinations Against Influenza A Virus Infections

In order to extend our findings beyond SARS-CoV-2, we tested IFNa2a-based combinations against FluAV. Through completion of a literature review, we identified several drugs that could be combined with IFNa2a to inhibit FluAV infection in vitro [10, 33, 34]. We tested emetine, flavopiridol, camostat, obatoclax, SNS-032, gemcitabine, monensin, cycloheximide and pimodivir against human influenza A/Udorn/307/1972 in A549 cells. Cell viability was measured after 48 h in FluAV- and mock-infected cells to determine compound efficiency and toxicity. We identified pimodivir as the most effective inhibitor of FluAV infection in vitro due to its ability to rescue cells from FluAV-mediated death at nanomolar concentrations, as well as its lack of detectable cytotoxicity up to 10 μM (Fig. 6a). IFNa2a rescued only portion of A549 cells from virus-mediated death at concentration of 40 ng/ml (Fig. 6b). We then tested antiviral activity and cytotoxicity of pimodivir-IFNa2a combination in FluAV-infected and mock-infected A549 cells using CTG assay. The drug combination was tested by a 6×6 dose-response matrix, where 5 doses of pimodivir and IFNa2a were combined in a pairwise manner. As a result, we obtained dose-response matrices demonstrating viability of FluAV- and mock-infected cells (Fig. 6c). We plotted

synergy distribution maps, showing synergy at each pairwise dose. We observed that IFNa2a-pimodivir combination was synergistic against FluAV infection (ZIP synergy score: 22.13, the most synergistic area score: 42.77) and was not toxic at synergistic doses for either drug. Given that pimodivir (VX-787, JNJ-63623872) is an orally available anti-FluAV agent which inhibits cap-snatching domain of viral polymerase basic protein 2 [35] and has shown promising results in Phase II clinical trials [36], we believe that its combination with IFNa warrants further preclinical and clinical investigations.

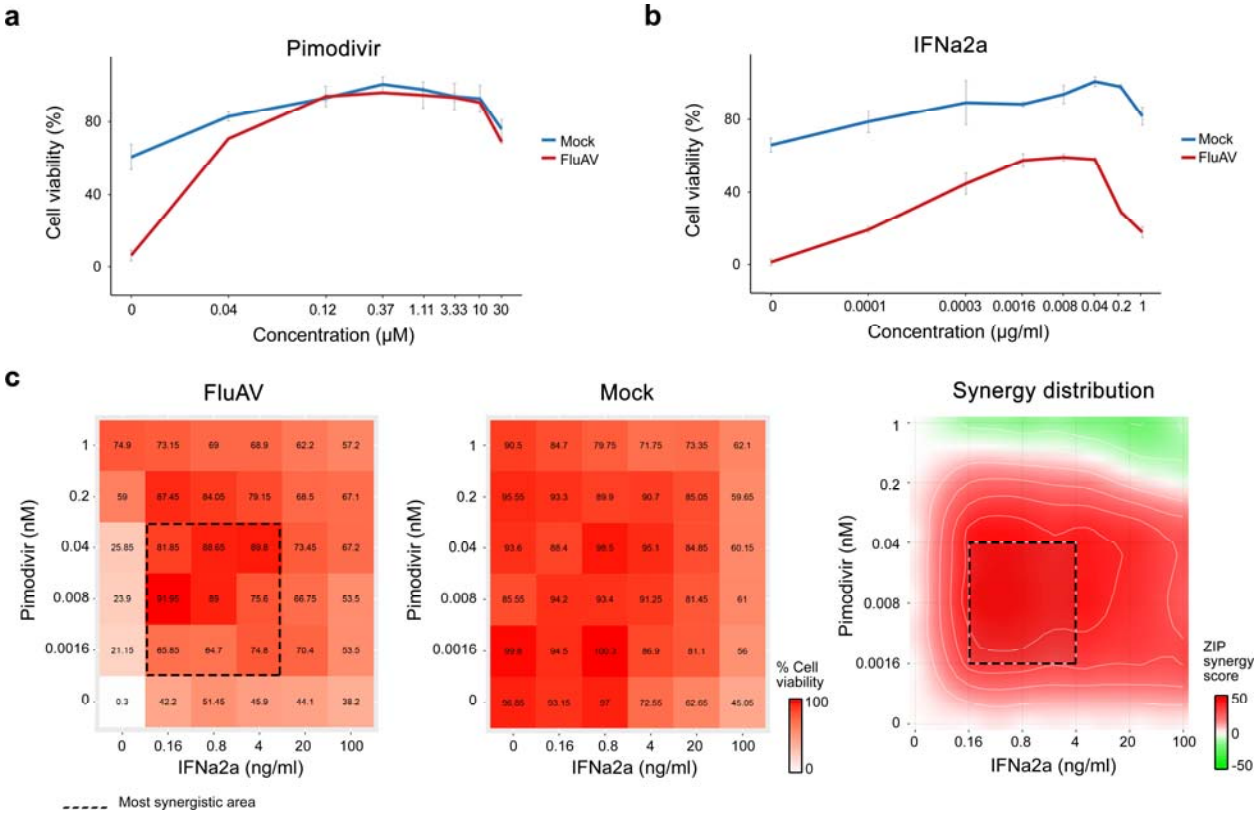

Figure 6. Combination of pimodivir-IFNa2a reduces FluAV infection in A549cells. (**a**,**b**) A549 cells were treated with increasing concentrations of pimodivir or IFNa2a and infected with the FluAV (moi = 0.5) or mock. After 48 h, cell viability was determined using a CTG assay. Mean ± SD; n = 3. (**c**) The interaction landscape of IFNa2a and pimodivir in FluAV- and mock infected A549 cells measured using CTG (left panels). The interaction landscape of both drugs showing synergy of the drug combination (right panel).

3.7. Novel IFNa2a-based Combinations Against Human Immunodificiency Virus 1 Infections

In order to further extend our findings beyond SARS-CoV-2 and FluAV, we tested IFNa2a-based combinations against HIV-1. Through literature review, we also identified several drugs that could be combined with IFNa2a to inhibit HIV-1 infection in vitro [37-40]. We tested brequinar, lamivudine, tenofovir, suramin, ezetimibe, minocycline, rapamycin, monensin, cycloheximide, clofarabine, fludarabine, cytochalasin d, pranlukast, decitabine and dexmedetomidine against a strain of HIV-1 that triggers expression of firefly luciferase upon infection in reporter TZM-bl cells. To determine compound efficiency, we measured HIV1-mediated firefly luciferase activity after 48 h in infected cells. We also determined toxicity of compounds in mock-infected cells using CTG. We identified 6 agents (lamivudine, brequinar, tenofovir, suramin, clofarabine and decitabine) which reduced HIV-1-mediated luciferase activity without detectable cytotoxicity. We tested combinations of IFNa2a with each of the above-stated antiviral agents to determine their effect on HIV-1-mediated increase in firefly luciferase expression in

TZM-bl cells. Five different concentrations of the compounds were added to virus- or mock-infected cells, either alone or in combination. Cell viability and HIV-induced luciferase expression were measured after 48 h. We identified that lamivudine and IFNa2a in combination was most effective while being nontoxic at synergistic drug concentrations, with ZIP synergy scores of 5.7 and ZIP synergy score of 11.4 at the most synergistic area (Fig. 7). Given that lamivudine (3TC) is an orally available anti-HIV drug which inhibits viral reverse transcriptase [41], we believe that its combination with IFNa also warrants further preclinical and clinical investigations.

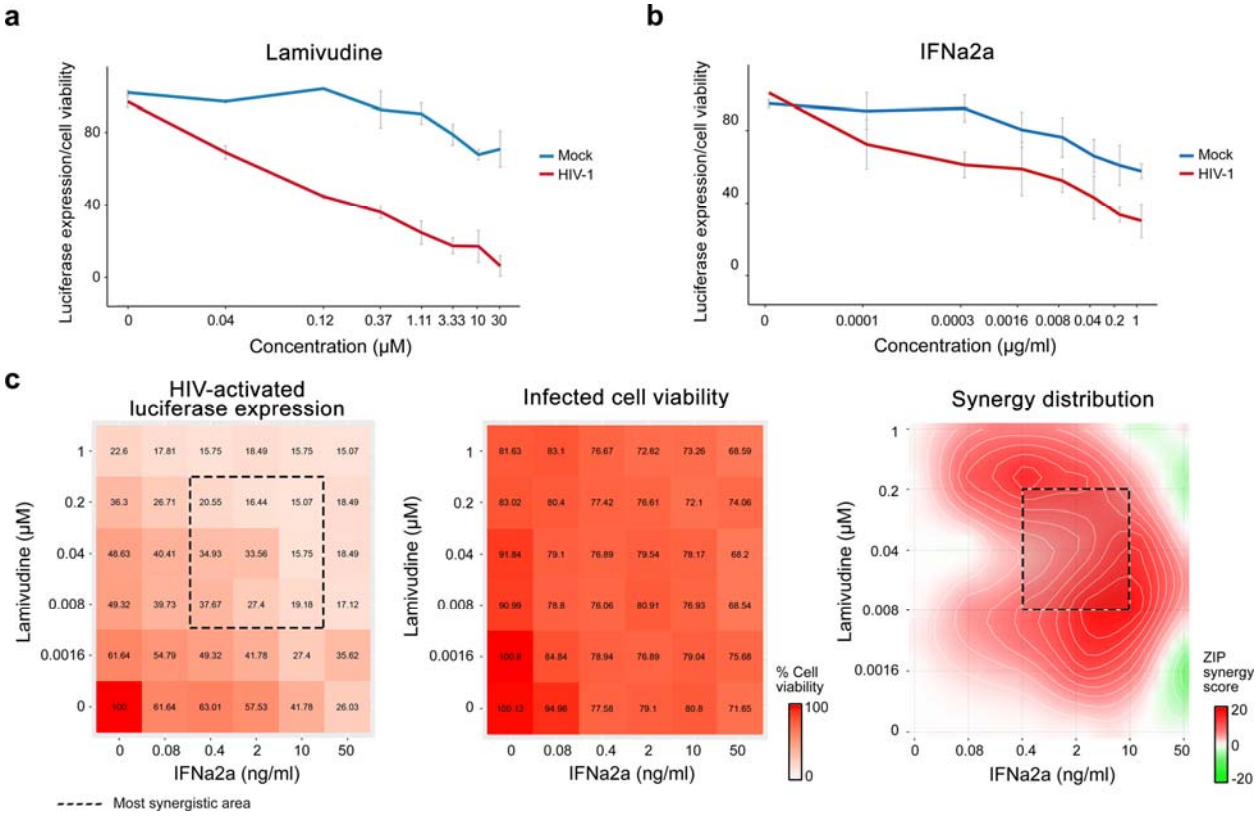

Figure 7. Combination of lamivudine-IFNa2a reduces HIV-1 infection in TZM-bl cells. (**a**,**b**) TZM-bl cells were treated with increasing concentrations of lamivudine or IFNa2a and infected with the HIV-1 or mock. After 48 h, the HIV-activated luciferase expression was measured (red curves). Viability of mock-infected cells was determined using the CTG assay (blue curves). Mean ± SD; n = 3. (**c**) The interaction landscape of IFNa2a and lamivudine measured using HIV-1-activated luciferase expression in HIV-1- and mock-infected TZM-bl cells, respectively (left panels). The interaction landscape of both drugs showing synergy of their combination (right panel).

4. Discussion

Although the use of antiviral drug cocktails is not new [42], monotherapy is mainly used at the moment to treat viral infections due to lack of studies on drug-drug interactions.. For example, remdesivir, hydroxychloroquine, lopinavir, and IFNb regimens have all been used on hospitalized patients with COVID-19 with no or limited efficacy, as indicated by overall mortality, initiation of ventilation, and duration of hospital stay [43, 44]. IFN-based cocktails could be efficacious against COVID-19 and other viral diseases, due to general and natural ability of IFNs to activate antiviral responses.

Here, we have reported several synergistic IFNa-based combinations that have better efficacy than single drug therapies. These combination treatments were able to reduce viral replication in vitro at lower concentrations than is required with monotherapies. The low effective doses of combination drugs may have several clinical advantages, including improved patient outcome and fewer adverse events associated with IFN-mediated hypercytokinemia, suppression of T-cell response, pain hypersensitivity, and behavior disturbance [21]. Moreover, depending on the existing body of knowledge around the antiviral added to IFNa, the most promising combinations may directly enter phase I/II clinical studies in cases of outstanding urgency, such as SARS-CoV-2 pandemic, allowing for a cheaper and faster path to market and widespread use.

In particular, we report novel anti-SARS-CoV-2 activities of IFNa2a in combination with remdesivir, EIDD-2801, camostat, cycloheximide, and convalescent serum in vitro. Because camostat-IFNa2a and convalescent serum-IFNa2a were the most synergistic combinations, we strongly urge further investigation into the combinations of these agents. The capacity to deliver camostat and IFNa2a through different routes could provide a path for effective treatment of COVID-19 patients at different stages of diseases [31, 45, 46]. Camostat may be of particular interest as it also possesses some potential beneficial immunomodulatory effects by interfering with the bradykinin/kallikrein pathways [47]. Moreover, due to the advanced developmental statuses of remdesivir and EIDD-2801 as antivirals, combinations of these drugs with IFNa2a can be also further investigated. Such combinations could be of relevance for patients with immune suppression including lymphopenia. Therefore, we urge that further clinical research on their use in combination with IFNa2a against SARS-CoV-2 is warranted.

We also identified synergistic activity in the combined administration of IFNa2a with the investigational drug pimodivir against FluAV, as well as in the combined administration of IFNa2a and lamivudine against HIV-1 infection. Both pimodivir and lamivudine are orally available drugs, while IFNs may be administered using various methods, including through aerosol inhalation. Because of this, these combinations may provide a relatively convenient treatment option that can be administered outside of a hospital setting. Thus, we believe further development of these combinations against FluAV and HIV-1 can lead to practical treatment options that are more effective while having potentially reduced side effects than currently existing treatments.

5. Conclusions

Here, we have identified novel synergistic IFNa-based combinations against SARS-CoV-2, FluAV and HIV infections in vitro. Our study indicates that lower and less toxic dosage of IFNa could be used when combined with other antivirals. Our next goal is to complete preclinical studies with the most effective and tolerable combinations and translate our findings into trials in patients. These combinations may have a global impact, improving the protection of the general population from emerging and re-emerging viral infections or co-infections, and allowing the swift management of immune-escaping viral variants and preventing development of drug-resistant viral strains.

Supplementary Materials: The following information is available online: Figure S1. Examples of IFN-based combinations and their developmental statuses. The data was retrieved from https://antiviralcombi.info database. Figure S2. Metabolomic analysis of mock- and SARS-CoV-2-infected Calu-3 cells non-treated or treated with type I IFNs. Figure S3. The effect of 6 drugs on SARS-CoV-2-mCherry-mediated expression of mCherry and virus-mediated death of Calu-3 cells. Figure S4. Effect of remdesivir, EIDD-2801, cycloheximide, and convalescent serum in combination with IFNa2a against SARS-CoV-2-mCherry infection in Calu-3 cells.

Author Contributions: All authors contributed to the methodology, software, validation, formal analysis, investigation, resources, data curation, writing, and review and editing of the manuscript. D.K. conceptualized, supervised, and administrated the study and acquired funding. All authors have read and agreed to the published version of the manuscript.

Funding: This research was funded by the European Regional Development Fund, the Mobilitas Pluss Project MOBTT39 (to D.K.). This work was financially supported by a National Research Foundation of Korea (NRF) grant funded by the Korean government (MSIT) (NRF-2017M3A9G6068246 and 2020R1A2C2009529). FIMM metabolomics unit was supported by HiLIFE and Biocenter Finland.

Acknowledgments: We thank personnel of Biomedicum function genomics (FuGu), Juho Vaananen and Martyn unit for transcriptomics analysis.

Conflicts of Interest: The authors declare no conflicts of interest.

References

1. Vos, T., et al., *Global, regional, and national incidence, prevalence, and years lived with disability for 328 diseases and injuries for 195 countries, 1990–2016: a systematic analysis for the Global Burden of Disease Study 2016.* The Lancet, 2017. **390**(10100): p. 1211-1259.
2. Hay, S.I., et al., *Global, regional, and national disability-adjusted life-years (DALYs) for 333 diseases and injuries and healthy life expectancy (HALE) for 195 countries and territories, 1990–2016: a systematic analysis for the Global Burden of Disease Study 2016.* The Lancet, 2017. **390**(10100): p. 1260-1344.
3. Fried, M.W., et al., *Peginterferon alfa-2a plus ribavirin for chronic hepatitis C virus infection.* N Engl J Med, 2002. **347**(13): p. 975-82.
4. Lazear, H.M., J.W. Schoggins, and M.S. Diamond, *Shared and Distinct Functions of Type I and Type III Interferons.* Immunity, 2019. **50**(4): p. 907-923.
5. Sallard, E., et al., *Type 1 interferons as a potential treatment against COVID-19.* Antiviral Res, 2020. **178**: p. 104791.
6. Sa Ribero, M., et al., *Interplay between SARS-CoV-2 and the type I interferon response.* PLoS Pathog, 2020. **16**(7): p. e1008737.
7. Park, A. and A. Iwasaki, *Type I and Type III Interferons - Induction, Signaling, Evasion, and Application to Combat COVID-19.* Cell Host Microbe, 2020. **27**(6): p. 870-878.
8. Felgenhauer, U., et al., *Inhibition of SARS-CoV-2 by type I and type III interferons.* J Biol Chem, 2020. **295**(41): p. 13958-13964.
9. Mesev, E.V., R.A. LeDesma, and A. Ploss, *Decoding type I and III interferon signalling during viral infection.* Nat Microbiol, 2019. **4**(6): p. 914-924.
10. Shim, J.M., et al., *Influenza Virus Infection, Interferon Response, Viral Counter-Response, and Apoptosis.* Viruses, 2017. **9**(8).
11. Zhang, Q., et al., *Inborn errors of type I IFN immunity in patients with life-threatening COVID-19.* Science, 2020. **370**(6515).
12. Hadjadj, J., et al., *Impaired type I interferon activity and inflammatory responses in severe COVID-19 patients.* Science, 2020. **369**(6504): p. 718-724.
13. Sancho-Shimizu, V., et al., *Inborn errors of anti-viral interferon immunity in humans.* Curr Opin Virol, 2011. **1**(6): p. 487-96.
14. Pairo-Castineira, E., et al., *Genetic mechanisms of critical illness in Covid-19.* Nature, 2020.
15. Sleijfer, S., et al., *Side effects of interferon-alpha therapy.* Pharm World Sci, 2005. **27**(6): p. 423-31.
16. Hung, I.F., et al., *Triple combination of interferon beta-1b, lopinavir-ritonavir, and ribavirin in the treatment of patients admitted to hospital with COVID-19: an open-label, randomised, phase 2 trial.* Lancet, 2020. **395**(10238): p. 1695-1704.
17. Idelsis, E.-M., et al., *Effect and safety of combination of interferon alpha-2b and gamma or interferon alpha-2b for negativization of SARS-CoV-2 viral RNA. Preliminary results of a randomized controlled clinical trial.* medRxiv, 2020: p. 2020.07.29.20164251.
18. Ianevski, A., et al., *Potential Antiviral Options against SARS-CoV-2 Infection.* Viruses, 2020. **12**(6): p. 642.
19. Ianevski, A., et al., *SynergyFinder: a web application for analyzing drug combination dose-response matrix data.* Bioinformatics, 2017. **33**(15): p. 2413-2415.
20. Ianevski, A., A.K. Giri, and T. Aittokallio, *SynergyFinder 2.0: visual analytics of multi-drug combination synergies.* Nucleic Acids Res, 2020. **48**(W1): p. W488-w493.

21. Gaelings, L., et al., *Regulation of kynurenine biosynthesis during influenza virus infection.* Febs j, 2017. **284**(2): p. 222-236.
22. Pichlmair, A., et al., *IFIT1 is an antiviral protein that recognizes 5'-triphosphate RNA.* Nat Immunol, 2011. **12**(7): p. 624-30.
23. Zhou, X., et al., *Interferon induced IFIT family genes in host antiviral defense.* Int J Biol Sci, 2013. **9**(2): p. 200-8.
24. Gusho, E., D. Baskar, and S. Banerjee, *New advances in our understanding of the "unique" RNase L in host pathogen interaction and immune signaling.* Cytokine, 2020. **133**: p. 153847.
25. Boergeling, Y. and S. Ludwig, *Targeting a metabolic pathway to fight the flu.* Febs j, 2017. **284**(2): p. 218-221.
26. Ritchie, M.E., et al., *limma powers differential expression analyses for RNA-sequencing and microarray studies.* Nucleic Acids Res, 2015. **43**(7): p. e47.
27. Bojkova, D., et al., *Proteomics of SARS-CoV-2-infected host cells reveals therapy targets.* Nature, 2020. **583**(7816): p. 469-472.
28. Sheahan, T.P., et al., *An orally bioavailable broad-spectrum antiviral inhibits SARS-CoV-2 in human airway epithelial cell cultures and multiple coronaviruses in mice.* Sci Transl Med, 2020. **12**(541).
29. Zhang, C.H., et al., *Antiviral activity of cepharanthine against severe acute respiratory syndrome coronavirus in vitro.* Chin Med J (Engl), 2005. **118**(6): p. 493-6.
30. Ko, M., et al., *Screening of FDA-approved drugs using a MERS-CoV clinical isolate from South Korea identifies potential therapeutic options for COVID-19.* bioRxiv, 2020: p. 2020.02.25.965582.
31. Breining, P., et al., *Camostat mesylate against SARS-CoV-2 and COVID-19-Rationale, dosing and safety.* Basic Clin Pharmacol Toxicol, 2020.
32. Ko, W.C., et al., *Arguments in favour of remdesivir for treating SARS-CoV-2 infections.* Int J Antimicrob Agents, 2020. **55**(4): p. 105933.
33. Söderholm, S., et al., *Multi-Omics Studies towards Novel Modulators of Influenza A Virus-Host Interaction.* Viruses, 2016. **8**(10).
34. Müller, K.H., et al., *Emerging cellular targets for influenza antiviral agents.* Trends Pharmacol Sci, 2012. **33**(2): p. 89-99.
35. Fu, Y., et al., *JNJ872 inhibits influenza A virus replication without altering cellular antiviral responses.* Antiviral Res, 2016. **133**: p. 23-31.
36. Finberg, R.W., et al., *Phase 2b Study of Pimodivir (JNJ-63623872) as Monotherapy or in Combination With Oseltamivir for Treatment of Acute Uncomplicated Seasonal Influenza A: TOPAZ Trial.* J Infect Dis, 2019. **219**(7): p. 1026-1034.
37. Andersen, P.I., et al., *Discovery and development of safe-in-man broad-spectrum antiviral agents.* Int J Infect Dis, 2020. **93**: p. 268-276.
38. Andersen, P.I., et al., *Novel antiviral activities of obatoclax, emetine, niclosamide, brequinar, and homoharringtonine.* Viruses, 2019. **11**(10): p. 964.
39. Ianevski, A., et al., *Expanding the activity spectrum of antiviral agents.* Drug Discov Today, 2019. **24**(5): p. 1224-1228.
40. Ianevski, A., et al., *Identification and Tracking of Antiviral Drug Combinations.* Viruses, 2020. **12**(10).
41. Perry, C.M. and D. Faulds, *Lamivudine. A review of its antiviral activity, pharmacokinetic properties and therapeutic efficacy in the management of HIV infection.* Drugs, 1997. **53**(4): p. 657-80.
42. *Antiviral Combination Database.* 2020 [cited 2020 Dec 31, 2020]; Available from: http://antiviralcombi.info/.
43. Pan, H., et al., *Repurposed Antiviral Drugs for Covid-19 - Interim WHO Solidarity Trial Results.* N Engl J Med, 2020.
44. Monk, P.D., et al., *Safety and efficacy of inhaled nebulised interferon beta-1a (SNG001) for treatment of SARS-CoV-2 infection: a randomised, double-blind, placebo-controlled, phase 2 trial.* Lancet Respir Med, 2020.
45. Rowe, S.M., et al., *Reduced sodium transport with nasal administration of the prostasin inhibitor camostat in subjects with cystic fibrosis.* Chest, 2013. **144**(1): p. 200-207.
46. Van Hoeven, N., et al., *Pathogenesis of 1918 pandemic and H5N1 influenza virus infections in a guinea pig model: antiviral potential of exogenous alpha interferon to reduce virus shedding.* J Virol, 2009. **83**(7): p. 2851-61.
47. Schmaier, A.H., *The contact activation and kallikrein/kinin systems: pathophysiologic and physiologic activities.* J Thromb Haemost, 2016. **14**(1): p. 28-39.